Mechanical Characterization of Wire Arc Additive Manufactured HSLA Steel

Luís Henriqure de Araújo Gonçalves
luis.h.goncalves@tecnico.ulisboa.pt

Instituto Superior Técnico, Universidade de Lisboa, Portugal

January 2021

Abstract

In the aerospace industry, there is a continuous demand for faster, cheaper, and more sustainable options. Additive manufacturing, more specifically Wire and Arc Additive Manufacturing, emerges as a viable competitor to more traditional methods, showing the great potential of being used in part production. This technique allows the creation of large geometry parts for a variety of materials. Some disadvantages are related to the poor mechanical performance and surface quality of the deposited material. However, a deeper understanding of this process is still needed as it remains fairly unexplored. In this work, HSLA steel WAAM wall structures were manufactured using two different heat inputs with the aim of studying its impact on the specimens' mechanical performance. Results showed that it had some influence on the specimen's mechanical performance, with the Lower Heat input set presenting a more refined microstructure and higher values of maximum strain and hardness. Little differences were spotted regarding the various specimen heights along the wall. Regarding fatigue life tests, and despite the small number of specimens tested, a large dispersion of results was observed. Phenomena such as secondary hardening may have contributed to this and future studies should focus on their investigation. Strain field measurement during the tensile tests with digital image correlation (DIC) allowed the verification of stress concentration areas in specific defects that led to the rupture of the specimens. These failure modes were verified in the fractography analysis and the mechanical behavior was compared with numerical models without the presence of defects.
Keywords: Additive Manufacturing, WAAM, mechanical performance, heat input

1. Introduction

In the aerospace industry, as well as other transport engineering sectors, there is a continuous search for cheaper, lighter and more sustainable materials that can present better or similar mechanical performances than the already existent ones. The techniques used to mold them are also a subject of constant improvement, with several options being presented to the manufacturers. New methods try to present ways of speeding up the manufacturing process and at the same time reducing the production costs and complexity, while keeping the same reliability.

Additive manufacturing (AM) has been experiencing an exponential growth in the past decades. Its cost-effective approach and versatility make it a strong candidate for many industrial applications. The ability to produce complex geometry parts and the range of materials that can be processed with it are the main strong points of this method category. However, its reliability and performance are still of big concern [1].

From the technologies used in the AM of metallic alloys, the most common ones are those based on laser. Laser metal deposition and selective laser melting are examples. Others, such as Wire and Arc Additive Manufacturing (WAAM), based on electric arc, have been investigated and are shown to be competitive with the first ones. Low fabrication times, ability to produce large geometry parts and low capital investment are just a few perks of this method [2]. A deeper understanding of this process is still in need.

This work studies the effect of the heat input and wall location on the mechanical properties of the specimens. These are subsequently correlated with microstructure observations. Fatigue lifetime and surface quality as well as mechanical performance of the produced parts require special attention. Additionally, certification of WAAM parts needs to be performed as it is slowing down a wider use of this technology [2].

2. Background

The WAAM process consists of building parts by staking layers of beads thanks to an electric

arc that melts a wire of the intended material [3]. This method can be used to produce large parts for several applications, such as aerospace, naval, and power generation, as well as to add details on existing parts originally manufactured through other processes. It is also useful to repair worn-out features or damaged parts by depositing new material on their surface, avoiding the need to produce a new part from scratch, resulting in significant cost savings. Being a relatively recent technology, it still faces many challenges. These included the presence of residual stresses, porosity, optimization of process parameters, deposition strategies, poor surface quality of the parts and standardization.

A smart strategy should be adopted with respect to the amount of Heat Input during the welding process. A higher input allows the deposition of more material but less with less accuracy, in what regards the quality of the surface. An exaggerated input will remelt the previously deposited layers, leading to a deterioration of the bead geometry, microstructure, and even affect the mechanical properties. In some extreme cases, it can cause the burn-off of the material and penetration of the substrate. Despite this, insufficient input also presents some setbacks: uneven deposition, unfused layers, and more spatter [4, 5].

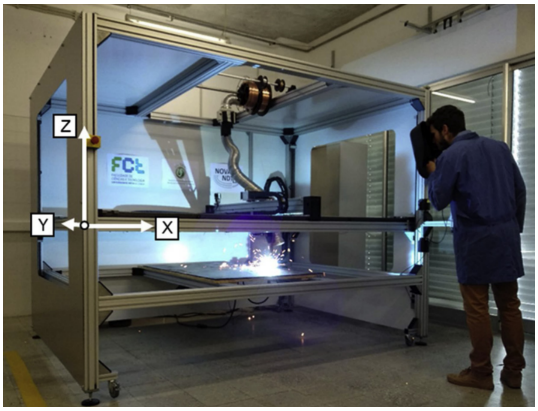

Figure 1: WAAM welding machine, adapted from [6].

It is also important to take into account the effect of the huge temperature difference between the bead and the substrate. This will cool down the molten metal before fine and uniform distribution of carbides takes place, leading to a columnar grain structure in the bead. Columnar grains typically grow in the building direction, perpendicular to the solid/liquid interface [7]. The main issue with this type of growth is the resulting anisotropic properties, which can be a major setback in multiaxial loading conditions. To diminish this, the preheating of the substrate is advised as it will ensure a decrease in the temperature gradient and help achieve a fine grain formation, and consequently leading to better mechanical properties [8, 9].

Rodrigues et al. [6] investigated the microstructure and mechanical properties of WAAM HSLA steel parts and their correlation with the heat input variation. In their observations, heat accumulation and consequent low cooling rates were shown to favour grain growth, meaning the parts built with a higher heat input presented larger grains, and the grain size increased along the height of the produced walls. Mechanical properties did not present any significant variations. The same phenomenon was documented by E. Aldalur et al. [10], with similar grain size variations being observed along the wall structure.

3. Experimental process development

3.1. Experimental Setup

The experimental apparatus used in this work was the custom-built WAAM-GMAW equipment existent in the industrial technology laboratories of FCT-UNL, see Figure 1, that consisted of a customized welding torch mounted on a three-axis positioning system, with a working envelope of 2760 x 1960 x 2000 mm. To deposit the material over the substrate, a welding machine from KEMPY, with a power source Pro MIG 3200, wire feeder, and control unit Pro MIG 501 was used. The mild steel substrates, where the walls were built on, had dimensions of 250 x 100 x 10 mm and were cleaned and dried before the experiment. The chosen wire material was a HSLA steel AWS A5.28 ER110S-G with a diameter of 1 mm. For the fatigue specimens walls a wire with a diameter of 1.2 mm was used due to lack of stock by the supplier. Table 1 presents its chemical composition.

Table 1: AWS A5.28 ER110S-G chemical composition [11].

C [%]	Si[%]	Mn [%]	P [%]	S[%]	Cu [%]
0.1	0.9	1.8	<0.015	<0.015	<0.25

Cr [%]	Ni [%]	Mo [%]	Al [%]	Zr + Ti [%]	Fe [%]
0.5	2.10	0.55	<0.10	<0.15	Balance

3.2. Specimen production

There were two different sets of walls produced, the first had a Low Heat (LH) input and the second a High Heat (HH) input. These were obtained by varying the travel speed of the process while the voltage, current, and wire feed speed were kept constant for both sets. Table 2 presents the values for these deposition parameters.

The walls produced had a length of 180 mm and the contact-tip-to-work distance was set to 7 mm. The dwell time between the deposited layers was kept constant at one minute. All experiments used a

Table 2: Process Parameters.

Sample	Voltage [V]	Current [A]	Wire Feed Speed [mm/s]	Travel Speed [mm/s]	Heat Input [J/mm]
LH	21	95	3	9	221
HH	21	95	3	3.9	511

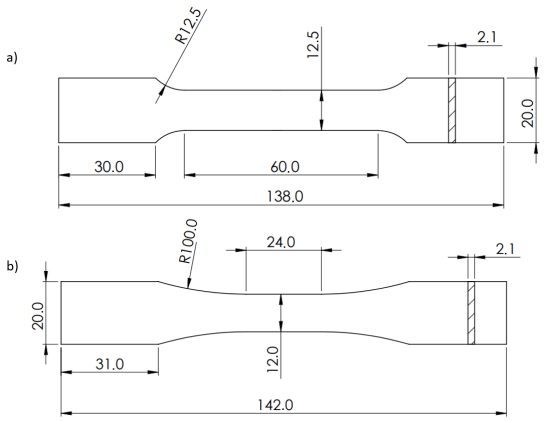

Figure 2: Specimen dimensions: a) tensile; b) fatigue.

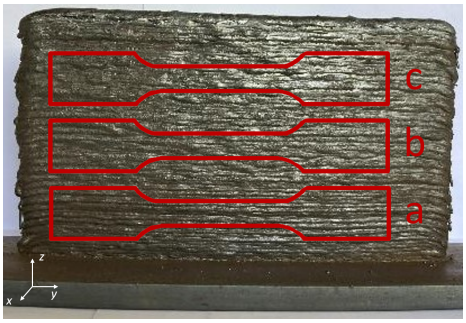

Figure 3: WAAM wall structure with specified specimen locations

continuous-wave mode with the electrode connected to the positive terminal (DC+).

The shielding gases used were pure Ar (99.999%) and a mixture of Ar + 1% CO2 + 18% He at a flow rate of 8 and 16 l/min for sets HH and LH, respectively. In the material deposition, for every layer deposited the torch ascended to a height equal to the bead height. The deposition strategy adopted was the zig-zag. This process was repeated until a height of approximately 100 mm was reached. These dimensions were specified in favour of the required number of tests and considering the fixture and the tool diameter. These parameters were based on previous similar works [6].

Specimens were obtained and shaped, see Figure 2, from the produced walls by Electrical discharge machining (EDM), according to the ASTM A370 standard. There were 3 different specimen locations: Base (a); Middle (b); and Top(c), see Figure 3.

In total, 27 specimens were produced and tested. 9 of them were subjected to fatigue tensile testing and the remaining 18 to tensile tests.

3.3. Characterization Techniques

For all tests and measurements performed, specimens from different Heat input sets as well as different wall locations were considered.

For the microstructural analysis, it was necessary to prepare the samples beforehand. These were cut, polished and contrasted with reagent (Nital 3%) to highlight grain boundaries and material constituents. The microscopy observation was conducted using the OLYMPUS CK40M microscope with increasing magnification values.

Vickers hardness was examined using the AVK-C2 Hardness Tester with an applied load of 2 kgf for 10 seconds, with a 1 mm distance separating each indentation.

Tensile tests were carried out at IST using the INSTRON® 3369 with 50 kN maximum load capacity. The cross-head speed was set to 1 mm/min. Displacement was measured either using a clip-gage, with an initial length of 25 mm, or the DIC equipment. For the latter, a special preparation was needed. A random pattern of points had to be created on the surface of the specimen by painting it with a white colour spray and then creating a random pattern with a black colour spray. This was so the cameras could follow the changes in surface strain distribution. The software used to process DIC images was VIC-2D 2009 and the camera used was the Allied Vision Stingray F504B.

Fatigue tests were carried out at IST using the INSTRON® 8502 machine. For all tests $R = \frac{\sigma_{min}}{\sigma_{max}} = 0.1$. These were ran until failure or if the run out criteria was reached, $N = 2 \text{ x } 10^6$ cycles. Frequency of the loads was either 12 or 15 Hz, and maximum stress applied was kept between 450 and 550 MPa.

A fractography analysis was performed using the Analytical SEM Hitachi S2400, at IST's MicroLab. Small samples from the fractured specimens of both tensile and fatigue trials were analysed with the aim of investigating their fracture surface and possible material imperfections.

FEM models were constructed to complement the

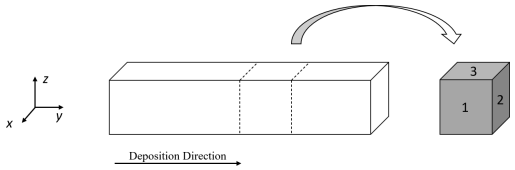

Figure 4: Scheme of the sample cut from a specimen (not at scale)

obtained results for the mechanical tests.

4. Results

4.1. Hardness

Hardness measurements were taken for Base and Middle specimens, for both Heat input sets. The results obtained demonstrated higher value of this parameter for the LH input set and for Base specimens. Hardness is directly related to the homogeneity of the microstructure, meaning higher grain refinement would increase its value. This does predict the presence of finer grains for the LH input set specimens, in comparison with HH input ones, and for the Base specimens. Higher heat build up and lower cooling rates experienced as the height of sample increases, and as the heat input changes from Low to High, can affect its microstructure and explain hardness values.

4.2. Microstructure

Observations were carried out for samples with Base and Middle locations, for LH and HH sets. Figure 3 shows a scheme with the samples' faces identified.

Consulting Figure 5, a clear difference between Low and High Heat input wall microstructures can be observed. Grain elongation is present for both cases, which is in agreement with literature reviews [5, 10], and fades away as the height increases due to the decreasing temperature gradient present. Grain refinement in LH input set is perceptibly higher than in HH input set due to lower heat build up and higher cooling rates. Differences in grain size between Base and Middle samples are not noticeable. These observations do not allow a definitive conclusion about the characteristics of the material's microstructure along the wall's height. Using a different reagent when contrasting the samples during their preparation, could be a possible solution to better distinguish the grains boundaries. Anisotropy was observed with face 3 of the samples exhibiting equiaxed grains instead of elongated.

4.3. Tensile Tests

Specimens belonging to the HH input set presented a significantly lower maximum strain when compared to the ones from the LH input set. This was directly related to the microstructural observations, where LH input set specimens evinced a more refined grain structure and hence presenting higher values for maximum strain.

For the different wall locations, in a first analysis, which considered all tested specimens (except 1La which ruptured for a very low strain), the outcome did not have a reasoned pattern and no conclusions could be drawn. Results from DIC tested specimens were isolated as a way to inquire if this more accurate strain measuring method could uncover any potential experimental errors. These maximum strain values presented little to no variation along the wall structure's height, evincing the previously observed microstructure homogeneity along wall height. In Figure 6, two graphs represent the maximum strain value for each heat input set and location.

Ultimate tensile strength was found to be similar between different Heat input sets. This parameter only showed a slight discrepancy regarding Base specimens, which presented a higher value in comparison to the others, see Figure 7. This is thought to be due to the marginal increase in grain refinement in this part of the wall which, by means of fine-grain strengthening mechanisms, inflated the value of UTS. When comparing the value of UTS for the wire material ($\sigma_U = 980$ MPa) with the mean values obtained (LH: $\sigma_U = 908.7$ MPa ; HH: $\sigma_U = 912.4$ MPa) it is safe to assume that the deposited material presents good strength. Toughness was found to have a similar variation to the maximum strain given that the values for UTS were very similar between specimens.

Regarding yield strength, the main point to be noted here is the large difference registered between the wire material ($\sigma_{yield} = 890$ MPa) and the deposited material ($\sigma_{yield} = 571.7$ MPa). The latter was not able to fulfill a decent approximation.

4.3.1 Specimen 1La

Results of tensile tests performed were presented and discussed, however, specimen 1La was not included. This suffered approximately 1/3 of the deformation to break, in comparison to others of the same category, due to a large amount of surface irregularities, in particular 3 evident surface voids.

Figure 8 a) shows a picture of the specimen in question and the three surface voids marked with red circles. In Figure 8 b) c) and d), the evolution of stress distribution in the material's surface is presented. To note that the painted surface, displayed in this image chain, is in the back of the one represented in Figure 8 a), so the concentration zones are expected to develop in a mirrored location.

The voids detected prior to the tensile loading are in fact the main causes of stress concentration in the specimen. Figure 8 b) shows two points of high stress concentration, corresponding to two void

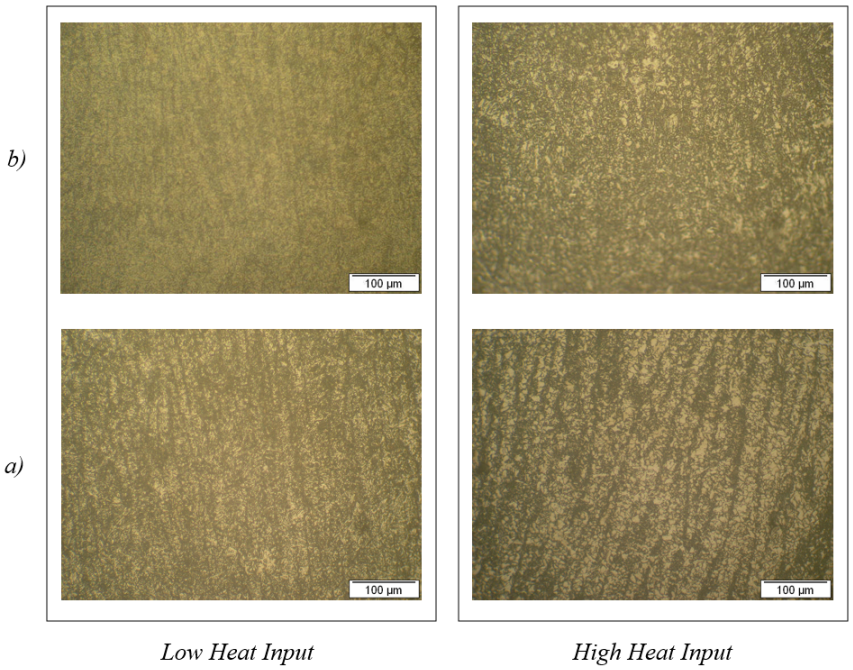

Figure 5: Microstructure (face 2): a) Base samples; b) Middle samples

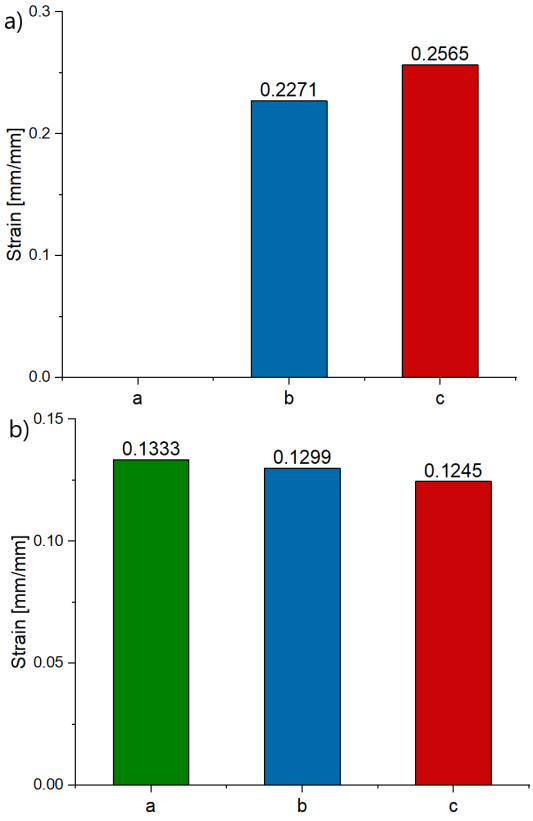

Figure 6: Bar plot representing maximum strain values for each height for specimens tested with DIC: a) for the LH input set; and for the HH input set.

locations the third one however, is evidently not present. This is because it is located on the edge of the specimen's surface which is not included in the software's area of interest. Nevertheless, stress distribution evolves into a single stress concentration area, Figure 8 c), which ultimately leads to rupture of the sample, Figure 8 d).

4.4. Fatigue Tests

These trials were performed under stress control and therefore belong to the High Cycle Fatigue (HCF) category. Fatigue life results were interpreted via an S-N curve, see Figure 9. Equation 1 evinces the approximation possible for the obtained values.

$$S = -13.44log(N) + 693.6, \quad R^2 = 0.0905 \qquad (1)$$

During fatigue testing, an unexpected occurrence took place as the specimens which were subjected to a maximum stress $\leq$ 510 MPa did not fail and reached the run out criteria ($N = 2$ x 10^6) while the ones subjected to a maximum stress $\geq$ 525 MPa failed much earlier than 2 x 10^6 cycles, the maximum being 160099 cycles to failure for specimen 10Lb. The explanations for this happening are not very clear. In literature, pre-straining of the material was found to induce considerable hardening and led to a significant discrepancy on fatigue life results. Major microstructural modifications were identified and described as secondary hardening, for HCF. This was characterized by a significant

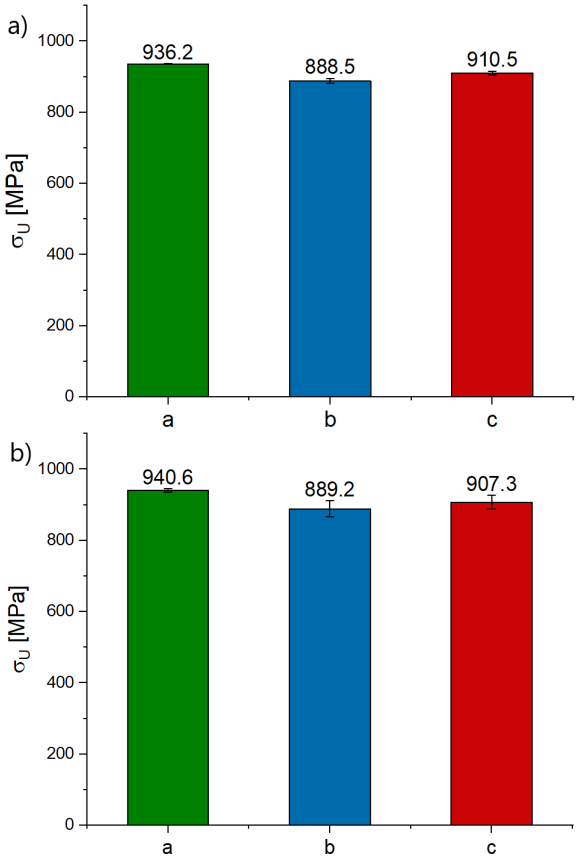

Figure 7: Bar plots representing σ_U values of each height for a) Low Heat Input; and b) High Heat Input.

cyclic hardening as well as extension of specimen fatigue life [12]. Different studies, not specifically about WAAM materials, using Low Cycle Fatigue and therefore being strain controlled tests, observed that in fact a secondary hardening, or secondary softening, phenomenon occured primarily due to certain strain amplitudes [13, 14]. The assessment of whether or not this is happening in the specimens tested stays out of scope of this study and should be analysed in future works.

4.5. Fractography Analysis

After the tensile and fatigue tests were finished, the most relevant specimens were chosen to be observed in the SEM, including 2La and 5Hc from tensile trials and 8Lb, 8Lc, 9La, 9Lc, 10Lb and 10Lc from fatigue trials.

Comparing the specimens from tensile tests, 2La (Low Heat input) presented a slightly more refined microstructure with smaller grain size than 5Hc (High Heat input). This goes in accordance with microstructural observations, regarding different heat input sets. When analysing fatigue specimens, there was a clear presence of striations, indicating that the specimen suffered a ductile fracture [15], see Figure 10 a) and b). This was more evident for specimen 10Lc. At the edge of the fracture surface, a secondary cracking occured. Here, rifling was also present showing again the ductility of the material, see Figure 10 c) and d). Also, images far from the fracture surface show a few black dots. These are thought to be microvoids resultant from the pullout of the grains, see Figure 10 e) and f). This is seen as a sign of an unstable rupture of this part of the specimen.

Samples chemical composition was also determined and did not present any unusual results, apart from the lack of Mo (0.5%).

5. Finite element analysis

In order to successfully simulate the tensile behaviour of the specimens, both elastic and plastic domains should be considered. For this, a structural analysis using *SOL 401 Multi-Step Nonlinear* with *Simcenter Nastran* solver was chosen. This simulation required the Young's modulus, Poisson's ratio and the values of the Stress vs. Strain curve of the material. Given that the Poisson ratio was not calculated during the experiments, it was assumed to be approximately $\nu = 0.3$, for steels [16]. Both the elastic modulus and the values of the Stress vs. Strain curve were changed according to the specimen being simulated. To note that the simulation only included part of the stress curve, until the ultimate tensile strength was reached.

After a mesh convergence study was performed, a 3D mesh was applied to the models with an element size of 1 mm and using CHEXA(20) elements, a 20-node three-dimensional element.

The numerical models constructed tried to emulate, as close as possible, the real tensile experiment parameters. A fixed constraint (encastrated) was applied to the bottom of the specimen and an enforced motion, in the yy direction, to the top of the specimen, see Figure 11.

Two specimens, 1Lc and 6Ha, were modeled and the overall results were fairly satisfactory, with the experimental behaviour of the specimens having a decent approximation to the finite element modeling.

Specimen 1Lc tensile test was performed with DIC as the strain measuring method. Given this, the comparison between numerical and experimental strain distribution could also be made visually.

After analysing and comparing Figures 12 a) and b), it is obvious that strain distribution is different between the two. In the FE simulation, the middle part of the specimen is all under similar values of strain, being this equally distributed. As for the experimental test, the middle section of the specimen presents some stress concentration areas where strain values are much higher than in the rest. This

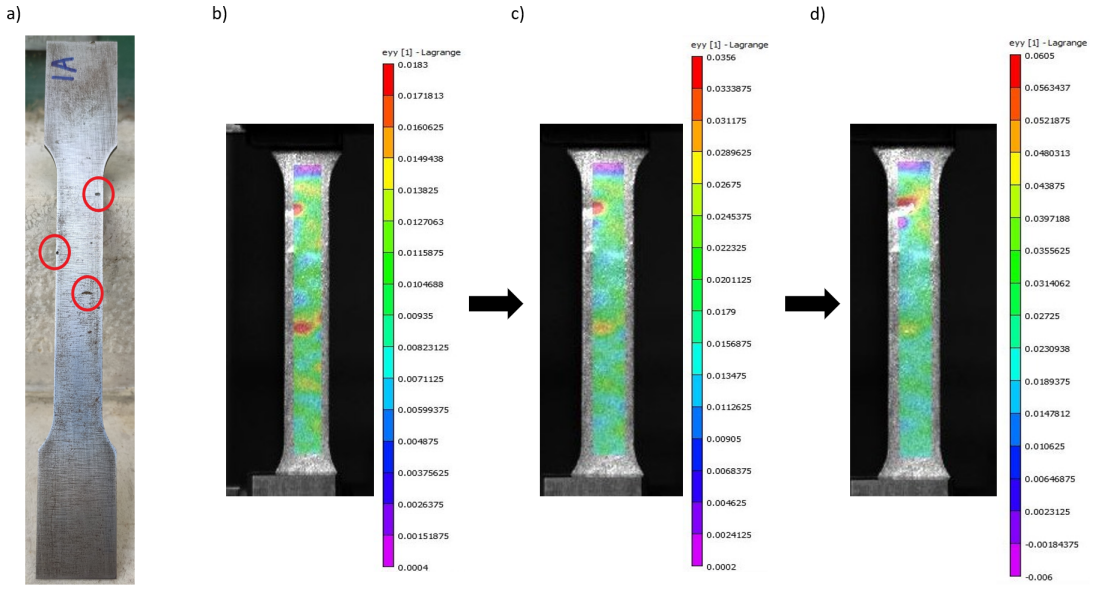

Figure 8: a) Specimen 1La with significant voids identified; Strain distribution along the surface of specimen 1La when: b) displacement equal to 1.594 mm; c) displacement equal to 2.273 mm; d) rupture occurs.

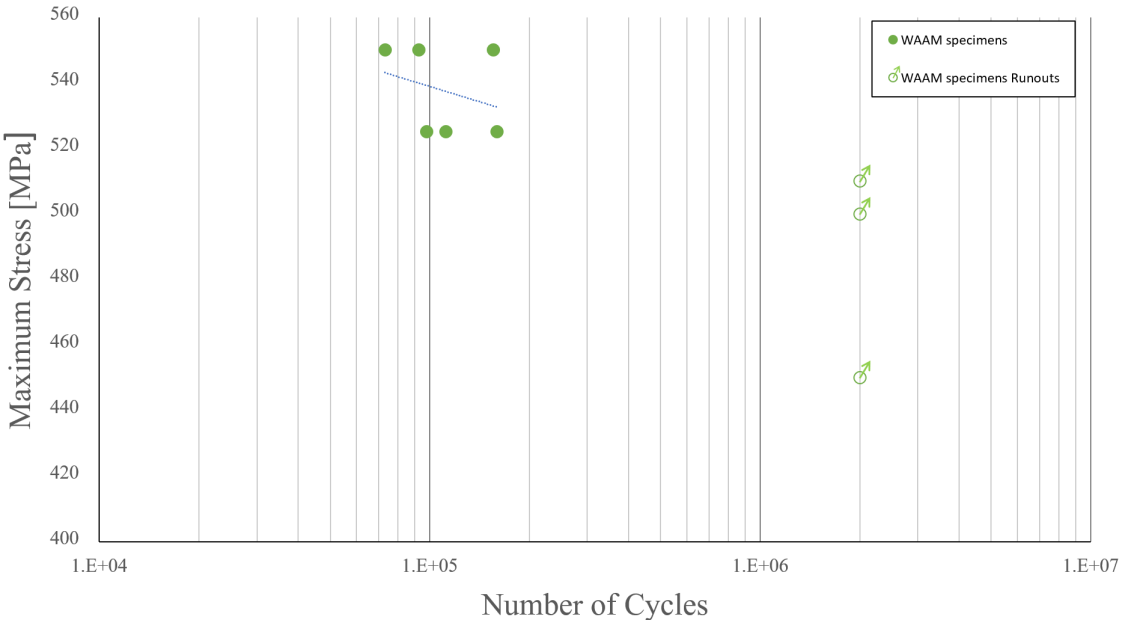

Figure 9: S-N curve of the tested WAAM specimens.

behaviour points to the existence of stress concentration features, such as porosity, roughness, etc, which will further affect the specimens tensile behaviour.

6. Conclusions

In this work, an investigation on the mechanical performance of WAAM specimens was conducted to better understand how the particular characteristics of this method would influence specimen's behaviour. Different heat input sets and specimen's height along the wall structure were compared for the various parameters accessed.

The following conclusions were drawn:

- Hardness values were higher for LH input samples and for Base samples, predicting a more refined grain structure for this Heat input and wall location;
- Heat input influenced the microstructure of the specimens. With LH input set presenting more refined grains in comparison with HH input set;

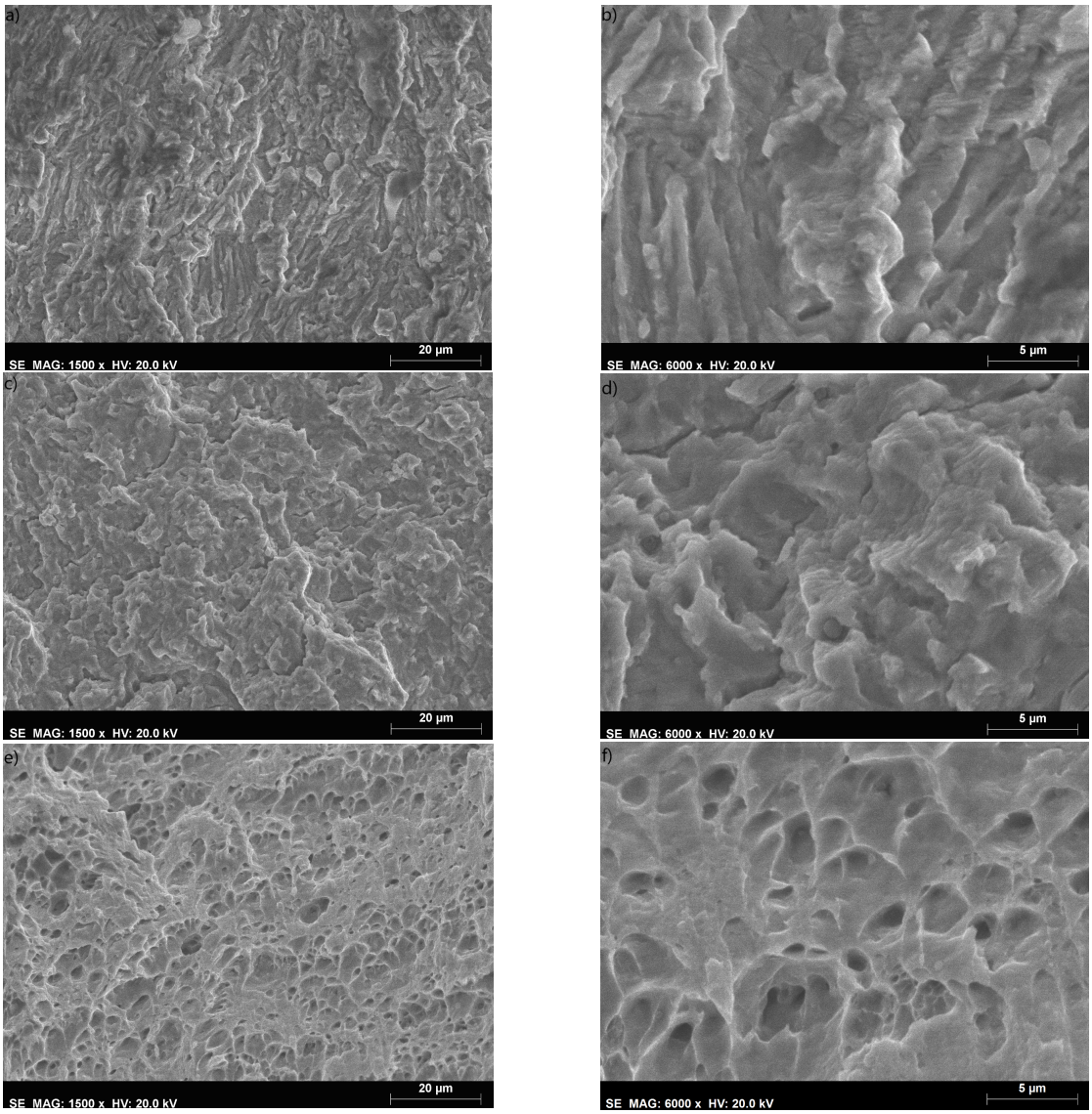

Figure 10: Detailed view of: specimen 10Lc microstructure at the primary fracture surface under an amplification of a) x1500; and b) x6000; specimen 10Lc microstructure at the secondary fracture surface under an amplification of c) x1500; and d) x6000; specimen 10Lc microstructure outside the fracture surface under an amplification of e) x1500; and f) x6000.

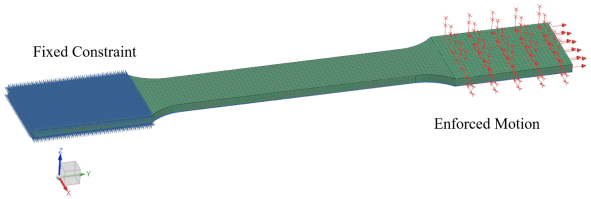

Figure 11: Boundary conditions on the simulated specimen.

- Specimen location did not significantly influence grain refinement, with no apparent changes being noticed;
- Samples, for both heat input sets, presented elongated grains, resultant from the temperature gradient. These faded away as the height of the sample increased;
- Maximum strain values were significantly higher for LH input specimen, which is related to their finer microstructure;
- UTS, for both Heat input sets presented a decent approximation to the wire material;
- Fatigue tests results, and despite the small number of specimens tested, presented a high level of dispersion, in terms of fatigue life, for the same load levels. Phenomena, such as secondary hardening, are believed to be the causes for this occurrence;

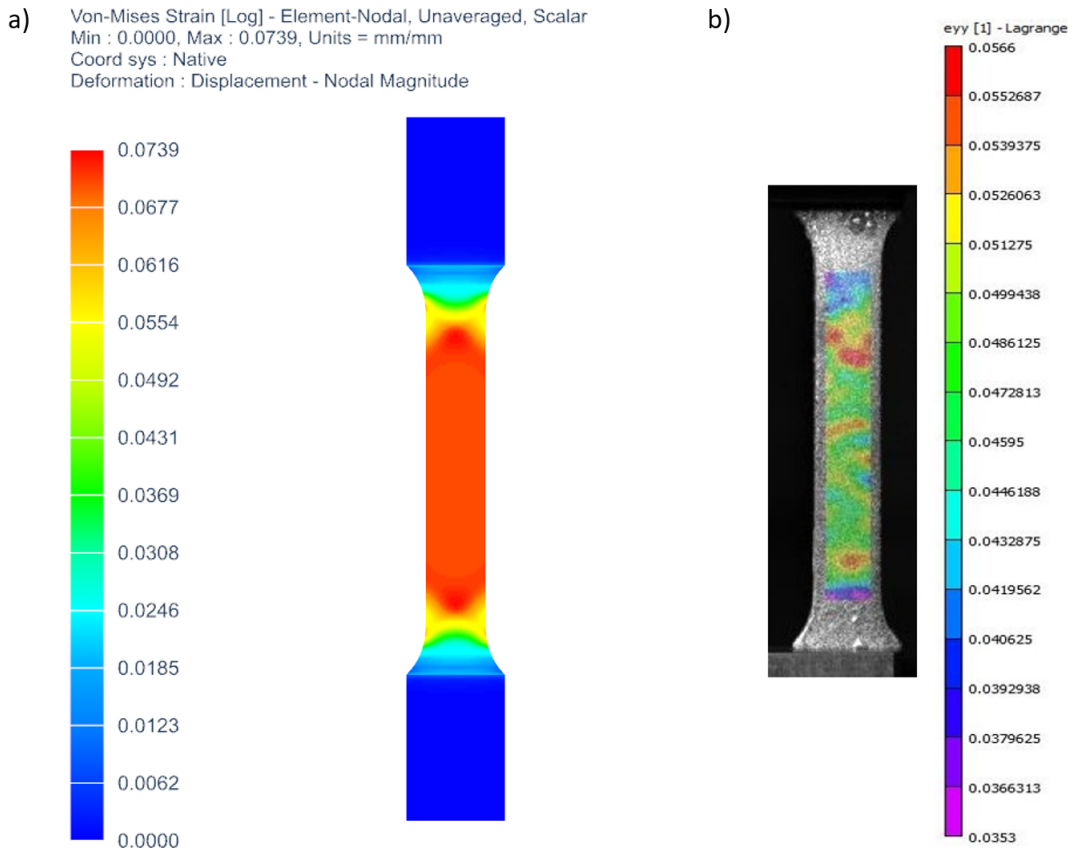

Figure 12: Strain distribution of specimen 1Lc for a displacement of approximately 4.916 obtained from: a) FEM model; b) DIC.

- Fractography analysis enabled the characterization of specimen fracture as ductile, due to the presence of striations;

- FEM models showed a good approximation between numerical and experimental results and helped to prove that stress distribution of tested specimens was clearly affected by material imperfections.

References

[1] T. Wohlers and T. Gornet. History of additive manufacturing. http://wohlersassociates.com/history2014.pdf. accessed: 14.12.2020.

[2] W. J. Sames, F. A. List, S. Pannala, R. R. Dehoff, and S. S. Babu. The metallurgy and processing science of metal additive manufacturing. *International Materials Reviews*, 61(5):315–360, 2016.

[3] C. Bourlet, S. Zimmer-Chevret, R. Pesci, R. Bigot, A. Robineau, and F. Scandella. Microstructure and mechanical properties of high strength steel deposits obtained by wire-arc additive manufacturing. *Journal of Materials Processing Tech.*, 285:1–13, 2020.

[4] M. Dinovitzer, X. Chen, J. Laliberte, X. Huang, and H. Frei. Effect of wire and arc additive manufacturing (WAAM) process parameters on bead geometry and microstructure. *Additive Manufacturing*, 26:138–146, 2019.

[5] J. C. G. Lopes. Feasibility of the milling process on HSLA parts manufactured with Wire and arc additive manufacturing. Master's thesis, Faculdade de Ciências e Tecnologia da Universidade Nova de Lisboa, 2019.

[6] T. A. Rodrigues, V. Duarte, J. A. Avila, T. G. Santos, R.M. Miranda, and J.P. Oliveira. Wire and arc additive manufacturing of HSLA steel: Effect of thermal cycles on microstructure and mechanical properties. *Additive Manufacturing*, 27:440–450, 2019.

[7] T. A. Rodrigues, V. Duarte, R. M. Miranda, T. G. Santos, and J. P. Oliveira. Current Status and Perspectives on Wire and Arc Additive Manufacturing (WAAM). *Materials*, 12(1121):1–41, 2019.

[8] S. R. Singh and P. Khanna. Wire arc additive manufacturing (WAAM): A new process to shape engineering materials. *Materials Today: Proceedings*, 2020.

[9] V. A. Hosseini, M. Högström, K. Hurtig, M. A. V. Bermejo, L. Stridh, and L. Karlsson. Wire-arc additive manufacturing of a duplex stainless steel: thermal cycle analysis and microstructure characterization. *Welding in the World*, 63:975–987, 2019.

[10] E. Aldalur, F. Veiga, A. Suarez, J. Bilbao, and A. Lamikiz. High deposition wire arc additive manufacturing of mild steel: Strategies and heat input effect on microstructure and mechanical properties. *Journal of Manufacturing Processes*, 58:615–626, 2020.

[11] Weldwire. Product Specification. http://www.weldwire.net/wp-content/uploads/2013/07/110S-G.pdf. accessed: 18.11.2020.

[12] J. Colin, A. Fatemi, and S. Taheri. Cyclic hardening and fatigue behavior of stainless steel 304l. *J Mater Sci*, 46:145–154, 2011.

[13] J. Zhou, Z. Sun, P. Kanouté, and D. Retraint. Experimental analysis and constitutive modelling of cyclic behaviour of 316l steels including hardening/softening and strain range memory effect in lcf regime. *International Journal of Plasticity*, 107:54–78, 2018.

[14] L. Xu, S. Yang, L. Zhao, Y. Han, H. Jing, and K. Wang. Low cycle fatigue behavior and microstructure evolution of a novel fe-22cr-15ni austenitic heat-resistant steel. *Journal of Materials Research and Technology*, 9:14388–14400, 2020.

[15] I. Dzioba and S. Lipiec. Fracture mechanisms of s355 steel—experimental research, fem simulation and sem observation. *Materials*, 12, 2019.

[16] The Engineering Toolbox. Poisson's Ratio. https://www.engineeringtoolbox.com/poissons-ratio-$d_1224.html.accessed$: 8.12.2020.